PCCP

PAPER

View Article Online
View Journal | View Issue

Cite this: *Phys. Chem. Chem. Phys.*, 2019, **21**, 14103

The effect of CO rotation from shaped pulse polarization on reactions that form C_2†

Hannah M. Ogden, [a] Tara J. Michael, [a] Matthew J. Murray, [b] Qingnan Liu, [c] Carlos Toro [a] and Amy S. Mullin *[a]

Received 7th November 2018,
Accepted 30th January 2019

DOI: 10.1039/c8cp06917d

rsc.li/pccp

The effect of CO rotational energy on bimolecular reactions to form electronically excited C_2 is reported here. The reactions are initiated by CO multiphoton absorption of 800 nm light in strong optical fields using two different polarization configurations based on shaped chirped pulses. The observation of Swan band emission indicates that $C_2(d^3\Pi_g)$ is a reaction product. The optical polarization is in the form of either an optical centrifuge or a dynamic polarization grating. In each case, the strong field aligns CO molecules and induces multiphoton absorption. Power-dependent measurements indicate at least seven photons are absorbed by CO; $CO(a^3\Pi)$ is a likely reactant candidate based on kinetic modeling. Relative reaction efficiencies are determined by measuring Swan band emission intensities. For a CO pressure of 100 Torr and an optical intensity of $I = 2.0 \times 10^{13}$ W cm^{-2}, the relative $C_2(d^3\Pi_g)$ yield with the dynamic polarization grating is twice that with the optical centrifuge. The extent of CO rotational energy was determined for both optical polarizations using high-resolution transient IR absorption for a number of CO states with $J = 62$–73 and E_{rot} up to 10 400 cm^{-1}. Optical centrifuge excitation generates at least 2.5 times more rotationally excited CO molecules per quantum state than the dynamic polarization grating. The results indicate that the effect of large amounts of CO rotational energy is to reduce the yield of the C_2 products.

Introduction

Optical fields have been used to influence chemical reactions by aligning and orienting molecules[1–8] and by preparing reactants with specific amounts of vibrational or electronic energy.[9–14] In the past several decades, a number of approaches have been used to prepare molecules with both low[15–18] and high[19–28] rotational energies but the role of rotational energy in bimolecular reactions has not been widely explored. Most such studies to date have focused on low rotational energies.[29–39] In some cases, rotational energy enhances reactive cross sections while in other cases the cross sections are reduced by rotational energy. Many factors appear to contribute including thermochemistry, steric effects, anisotropic potential energy surfaces, centrifugal barriers in entrance channels, and rotational adiabaticity.[29–39] Here we investigate how bimolecular reactions are affected when reactant molecules have large amounts of rotational energy that are well beyond typical energies in a thermal ensemble.

In this study, we use strong optical fields based on shaped chirped pulses of 800 nm light. The shaped pulses excite CO through multiphoton absorption and C_2 Swan band emission is observed, evidence that electronically excited C_2 molecules are formed from excited CO. We control the polarization of the pulsed light to either have angular acceleration or form a dynamic polarization grating. The angularly accelerating field is an optical centrifuge and is capable of preparing CO molecules with oriented angular momentum in rotational states up to $J = 73$ with $E_{rot} \approx 10\,400$ cm^{-1}. The dynamic polarization grating has a time-varying polarization that changes from linear to elliptical to circular and then back to linear within an optical cycle. The dynamic polarization grating does not impart appreciable torque to the aligned CO molecules. Using these two polarization schemes, we compare the Swan band emission characteristics to elucidate the role of rotation in reactions that form C_2.

We have used the optical centrifuge to observe previously unseen IR transitions of high-J molecules and to study the collision dynamics of molecules with large amounts of oriented angular momentum.[21–27] More recently we have developed the tools to measure the time-dependent anisotropy of optically centrifuged molecules, and to investigate how atomic buffer gases affect the relaxation dynamics of centrifuged molecules.[26,27] Corkum and co-workers first demonstrated that the optical centrifuge was capable of dissociating Cl_2 through rotational excitation.[19] In other work, the Milner group has used coherent Raman spectroscopy to observe excitation and subsequent rotational revivals of N_2O molecules in an optical centrifuge.[28]

[a] *Department of Chemistry and Biochemistry, University of Maryland, College Park, MD, 20742, USA. E-mail: mullin@umd.edu*
[b] *Naval Research Laboratory, Washington DC, 20375, USA*
[c] *National Institute of Standards and Technology, Gaithersburg, MD, 20899, USA*
† Electronic supplementary information (ESI) available. See DOI: 10.1039/c8cp06917d

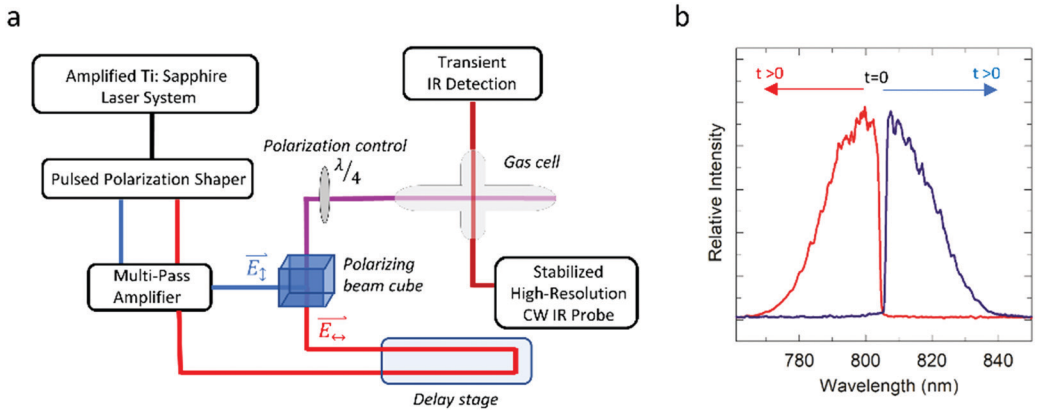

Fig. 1 (a) Schematic of experimental set up. An amplified Ti:sapphire laser system is spectrally divided into two pulses in a polarization shaper. The two pulses are then amplified with a multi-pass amplifier and combined with a polarizing beam cube. Stabilized high-resolution CW IR probe is used to measure transient population of specific rotational states. (b) Spectral output of the polarization shaper.

Here we study the effect that rotational energy has on bimolecular reactions initiated by strong optical fields with controlled polarization. The remainder of this paper describes our experimental approach and presents our results. Power-dependent C_2 emission spectra are reported, providing information about the multiphoton nature of the CO excitation. A mechanism for production of C_2 is proposed based on known kinetic and photophysical data for CO. The extent of rotational excitation in CO is reported for both polarization configurations based on high-resolution transient IR absorption measurements. Relative reaction efficiencies are reported based on the observed emission intensities and finally the role of reactant rotational energy is discussed.

Experimental methods

Two polarization configurations of the pulsed 800 nm light are used in these experiments: optical centrifuge polarization (OCP) and a dynamic polarization grating (DPG). Both optical polarizations are based on pairs of oppositely chirped pulses that are merged using a polarizing beam cube, then overlapped in time and space at the sample cell.

The instrumentation used to generate the pulses in this experiment has been described in detail previously.[21–27] Fig. 1a shows the essential components of the experiment. An optical pulse centered at λ_0 = 805 nm with a 40 fs pulse length is generated by a Ti-Sapphire ultrafast laser (Coherent). The pulse is stretched in time to 100 ps, amplified at a repetition rate of 10 Hz and given a positive chirp of $\Delta\lambda = -35$ nm based on the full-width-at-half-maximum (FWHM) of the spectral bandwidth. The pulse is spatially dispersed with a grating and split at λ_0 = 805 nm to form a pair of chirped pulses. The pulse with $\lambda > 805$ nm is turned into a negatively chirped pulse with a second grating. Each pulse is then spatially recombined by an additional grating.

Fig. 1b shows the spectral profiles of the pair of oppositely chirped pulses and indicates the direction of both linear chirps. The combined energy of the pair of pulses is increased to 45 mJ per pulse with a multi-pass amplifier pumped by the second harmonic of a Nd:YAG laser (Continuum). The pulses emerge from the multi-pass amplifier with linear p-polarization and opposite spectral chirp. A half-wave ($\lambda/2$) plate flips the polarization of one of the pulses to s-polarization, as shown in Fig. 2a. The pair of pulses are recombined spatially in a polarizing beam cube and sent through a quarter-wave ($\lambda/4$) plate. This induces opposite circular polarization in the pair of pulses and creates the optical centrifuge. For the dynamic polarization grating, the quarter-wave plate is removed, and the pair of pulses have orthogonal

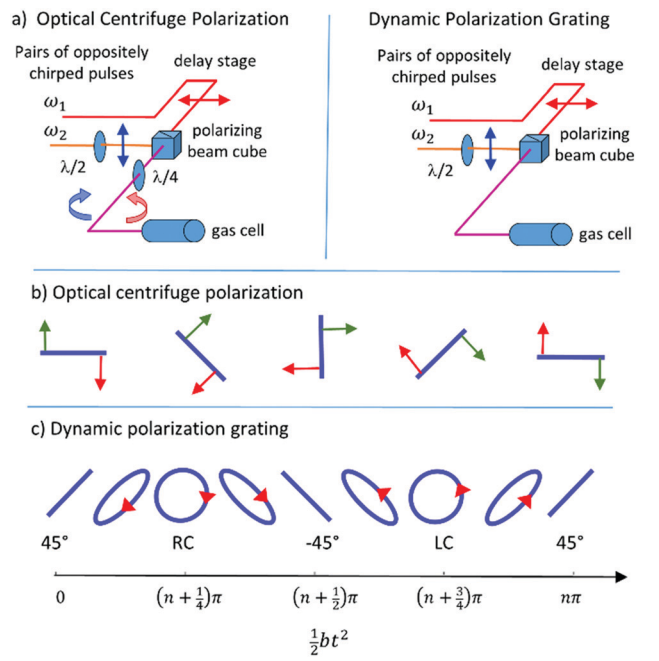

Fig. 2 (a) Experimental setup for generating light with optical centrifuge polarization and a dynamic polarization grating. (b) The optical centrifuge has linearly polarized light that angularly accelerates over the time of the pulse. (c) The dynamic polarization grating changes polarization from 45° linear, to right circular, to −45° linear, to left circular and back to 45° linear.

linear polarization. The resulting polarization configurations are described in detail in the section below.

The recombined pulses are focused to a beam waist of ω_0 = 53 μm at the centre of a Pyrex sample cell containing spectroscopic grade CO gas (99.99% purity) at pressures of 25, 50, 75 or 100 Torr. In this study, the intensity of the optical field ranges from 3.6×10^{12} W cm^{-2} (8 mJ per pulse) to 2.0×10^{13} W cm^{-2} (44 mJ per pulse).

Two types of measurements were performed with each polarization configuration. In the first, dispersed Swan band emission between λ = 400–800 nm was collected on an Ocean Optics 2000 spectrometer (1.5 nm FWHM) positioned at right angles to the pulsed laser propagation vector. The dispersed emission was collected as a function of pressure and power.

In the second type of measurement, high-resolution transient IR absorption signals were collected in a multipass cell (with 11 passes) for a number of CO ($X^1\Sigma^+$, v = 0) rotational states with J = 62–73 using polarization-sensitive IR spectroscopy. These measurements are used to establish the extent of rotational excitation in the CO sample with the optical centrifuge and with the dynamic polarization grating. A single-mode quantum cascade laser (Daylight Solutions) operating at λ = 4.3 μm with frequency resolution of $\Delta\nu_{IR} < 2 \times 10^{-4}$ cm^{-1} was tuned to the frequency of individual transitions and transient absorption was measured using an InSb detector with a rise time of 35 ns. This technique is described in detail elsewhere.[24–27]

Polarization of shaped pulsed light

In general, the oscillation of an optical field that propagates in the z-direction and starts at frequency ω_0 can be written as

$$\cos(\omega_0 t + \varphi(t) - kz) \quad (1)$$

where $\varphi(t)$ is a phase shift. The instantaneous frequency is given by

$$\omega(t) = \frac{d}{dt}(\omega_0 t + \varphi(t)) \quad (2)$$

If there is a time-dependent phase shift of $\varphi(t) = \frac{1}{2}bt^2$, then the pulse has a linear frequency chirp where b is the chirp rate. In the OCP, oppositely chirped pulses with right and left circular polarization are combined with no initial phase shift and the net result for the optical field oscillation is

$$\left(x\cos\left(\frac{1}{2}bt^2\right) + y\sin\left(\frac{1}{2}bt^2\right)\right)\cos(\omega_0 t - kz) \quad (3)$$

This is an instantaneously linearly polarized field that oscillates at an average frequency ω_0 but with a polarization that spins at angular frequency $bt/2$, *i.e.* at an ever-increasing rate during the pulse. The accelerating angular frequency is responsible for spinning molecules that are aligned in the field to high rotational states. Fig. 2b shows that the electric field for this situation rotates a complete cycle for π radians of $\frac{1}{2}bt^2$.

For the DPG, oppositely chirped pulses with orthogonal linear polarization are combined and the resulting field oscillation is written as

$$\frac{x+y}{2}\cos(\omega_0 t - kz)\cos\left(\frac{1}{2}bt^2\right) - \frac{x-y}{2}\sin(\omega_0 t - kz)\sin\left(\frac{1}{2}bt^2\right) \quad (4)$$

This is a combination of two linear fields at 45° and −45°. Any time that $\frac{1}{2}bt^2 = n\pi$, the sine of this argument is zero and the overall field is 45°. Similarly, when $\frac{1}{2}bt^2 = \left(n+\frac{1}{2}\right)\pi$, the polarization is −45°. If $\frac{1}{2}bt^2 = \left(n+\frac{1}{4}\right)\pi$, the field is left circularly polarized and if $\frac{1}{2}bt^2 = \left(n+\frac{3}{4}\right)\pi$, the field is right circularly polarized. At times in between, the field is elliptically polarized. Fig. 2c shows that the DPG field undergoes a complete cycle over π radians of $\frac{1}{2}bt^2$. Again, the base oscillation is at ω_0 and the polarization cycling frequency is $bt/2$.

A key difference between the OCP and DPG is the molecular response to the changing polarization. Molecules aligned in the optical centrifuge are spun into high rotational states by the angularly accelerating field. Molecules aligned in the dynamic polarization grating oscillate with the field but are not rotationally accelerated by the time-dependent optical polarization.

Results and discussion

Here we present the results of power- and pressure-dependent dispersed emission measurements when CO is excited by a strong optical field with the two different optical polarization. We analyse the multiphoton absorption of CO and consider the pathways that are likely to lead to C_2 formation. For both optical polarizations, the extent of CO rotational energy is characterized by high-resolution transient IR absorption and the influence of rotation on the bimolecular reactions is discussed.

Dispersed emission measurements: C_2 formation

Fig. 3 shows power-dependent emission spectra observed in a 100 Torr sample of CO. The spectra are identified as the well-known C_2 Swan bands ($d^3\Pi_g \rightarrow a^3\Pi_u$).[40–47] The Swan band peaks correspond to different vibronic transitions from the excited $d^3\Pi_g$ state: the Δv = 0 peak is at λ = 516 nm and the Δv = −1 peak is at λ = 467 nm. Interestingly, no emission from the CO Angstrom bands ($B^1\Sigma^+ \rightarrow A^1\Pi$) was seen in our measurements.[48] The lack of observed emission is consistent with a short-lived CO $B^1\Sigma^+$ state that is collisionally quenched, given the pressures used in our experiments. The kinetics will be considered in more detail in a later section.

The observation of Swan band emission from a pure sample of CO is evidence that excited $C_2(d^3\Pi_g)$ is a reaction product

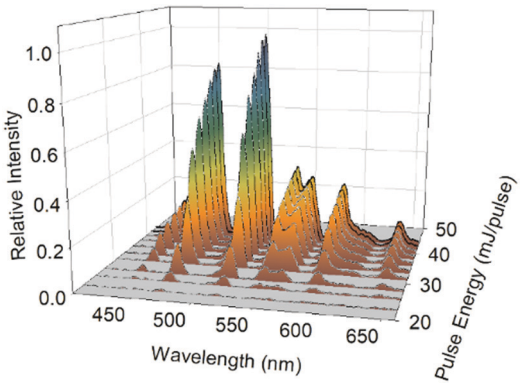

Fig. 3 Power-dependent Swan Band emission spectra at a cell pressure of 100 Torr and optical centrifuge polarization.

when CO is excited in an intense laser field. The emission intensity is a measure of the $C_2(d^3\Pi_g)$ yield. Fig. 4a–d show the power-dependent integrated emission at four CO pressures, ranging from 25 to 100 Torr, for both optical polarizations.

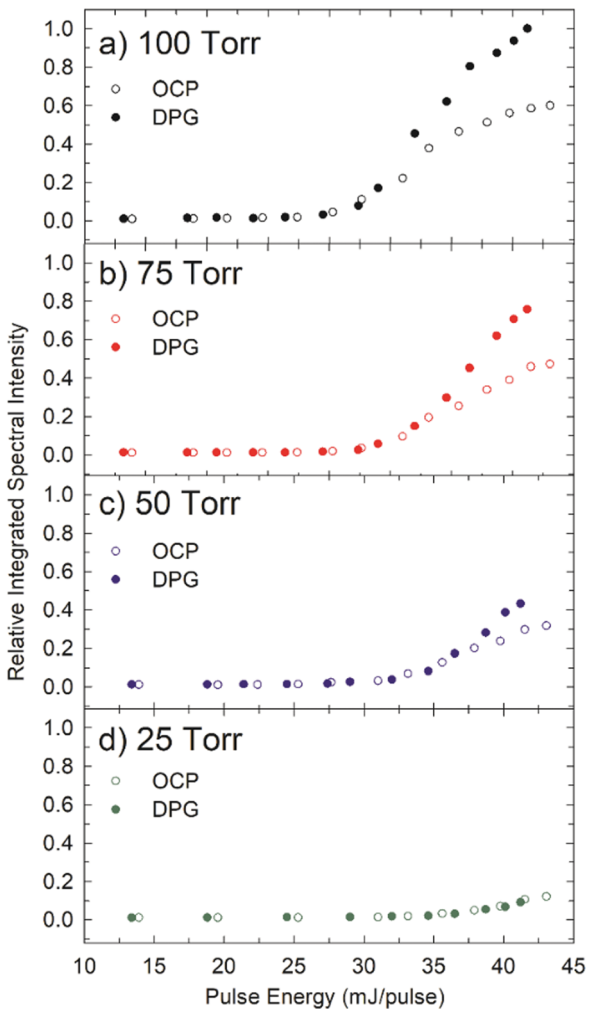

Fig. 4 Relative integrated spectral intensities at pressures of (a) 100 Torr, (b) 75 Torr, (c) 50 Torr, and (d) 25 Torr with either the optical centrifuge polarization (OCP) or dynamic polarization grating (DPG) polarizations.

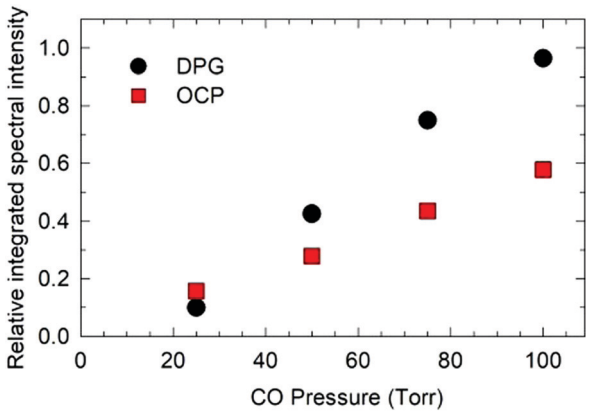

Fig. 5 Comparison of relative integrated C_2 emission intensity for optical centrifuge polarization (OCP) and the dynamic polarization grating (DPG) as a function of cell pressure with $I = 1.8 \times 10^{13}$ W cm^{-2} (41 mJ per pulse).

The emission threshold decreases with increasing pressure. Above threshold, the emission intensity increases with increasing laser power and for pressures of 50–100 Torr, there is more emission for the DPG than the OCP at the higher powers.

Fig. 5 shows a comparison of the relative integrated C_2 emission intensity for the OCP and DPG configurations as a function of cell pressure with $I = 1.8 \times 10^{13}$ W cm^{-2} (41 mJ per pulse). The difference in emission for the two optical polarizations increases with increasing pressure from 50 to 100 Torr. At 100 Torr and the highest pulse energies, the DPG leads to nearly twice the emission of the OCP. This observation shows that the DPG is twice as effective at converting CO to $C_2(d^3\Pi_g)$ under these conditions.

Multiphoton absorption of CO

The multiphoton absorption of CO is characterized using the linear portions of the energy-dependent data in Fig. 4. Fig. 6 shows the log–log plots and their linear fits for both optical polarizations. The slopes from the fitting analysis are listed in Fig. 6 and indicate that CO absorbs at least seven photons prior to the formation of C_2. The energy of seven 800 nm photons is enough to excite CO to the $B^1\Sigma^+$ state, as indicated by the red arrow in the energy level diagram (Fig. 7).[40] Absorption of eight photons would excite CO to the $F^1\Sigma^+$ state.

Mechanism of C_2 formation

Here we consider the mechanism by which C_2 is formed following the multiphoton absorption of CO. In 1981, C_2 Swan band emission was reported by Faust and coworkers after multiphoton UV excitation of CO.[41] Their time-resolved emission data indicate the presence of a long-lived precursor to the formation of C_2 from excited CO. In 1991, Ivanov and coworkers identified the CO $a^3\Pi$ state as important in the production of C_2 in CO/He plasmas. They report a relatively slow rate constant of $k_a = 10^{-12}$ cm^3 molecule^{-1} s^{-1} for the reaction of triplet CO with ground state CO, as shown in eqn (5).[49]

$$CO(a^3\Pi) + CO(X^1\Sigma^+) \xrightarrow{k_a} CO_2 + C \qquad (5)$$

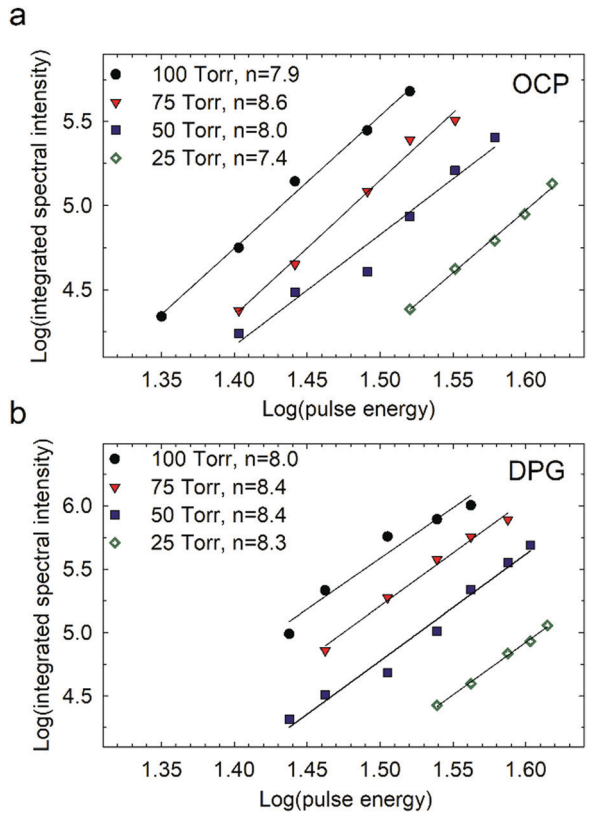

Fig. 6 Power-dependent analysis to determine the lower limit for the number of photons absorbed by CO that initiate formation of $C_2(d^3\Pi_g)$. Log–log plots of integrated spectral intensity *vs.* pulse energy for (a) the optical centrifuge polarization and (b) the dynamic polarization grating.

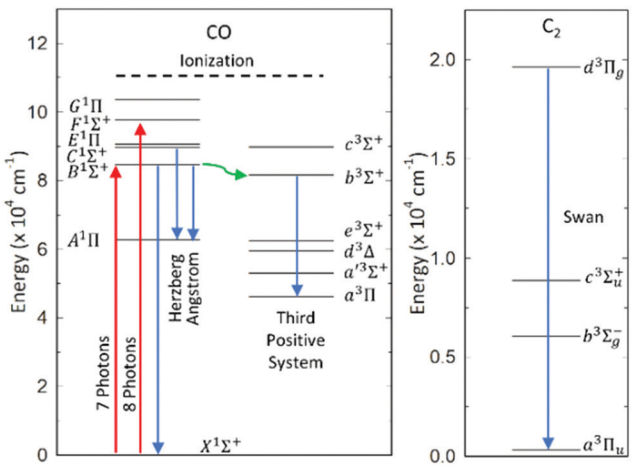

Fig. 7 Electronic energy levels and terms for CO and C_2. The red arrows indicate multiphoton absorption of seven and eight 800 nm photons. Emission is indicated with blue arrows and collision-induced intersystem crossing (denoted in green) leads to excitation of CO triplet states.

They postulate that the formation of C_2 then occurs by reactions of $CO(a^3\Pi)$ and a C atom, as in eqn (6).

$$CO(a^3\Pi) + C \xrightarrow{k_b} C_2 + O \quad (6)$$

It is likely that the rate constant for the second reaction is fast compared to the production rate of C atoms.

The CO $a^3\Pi$ state is a likely reactant in C_2 formation, based on the CO/He plasma studies discussed above. Here we consider the kinetics of the CO $B^1\Sigma^+$ state that is prepared by multiphoton absorption and ultimately leads to formation of the CO $a^3\Pi$ state. Both radiative decay and collisional energy transfer are included in the kinetics. If higher energy CO states are prepared in the initial multiphoton step, it is likely that the relaxation will be even faster.

We treat the initial multiphoton excitation of CO as prompt, since the highest pulse intensity occurs early in the shaped pulses. In this analysis, we begin with initial excitation to the B state, as shown in eqn (7) and Fig. 7. The B state can relax by emission to the X and A states (eqn (8)) and by collision-induced intersystem crossing to the CO $b^3\Sigma^+$ state (eqn (9)). The $b^3\Sigma^+$ state can relax by emission (eqn (10)) and by collisions to the $a^3\Pi$ state (eqn (11)).

$$CO(X^1\Sigma^+) + h\nu \xrightarrow{\text{prompt}} CO(B^1\Sigma^+) \quad (7)$$

$$CO(B^1\Sigma^+) \xrightarrow{k_1} \{CO(A^1\Pi) \text{ or } CO(X^1\Sigma^+)\} + \text{photon} \quad (8)$$

$$CO(B^1\Sigma^+) + M \xrightarrow{k_2} CO(b^3\Sigma^+) + M \quad (9)$$

$$CO(b^3\Sigma^+) \xrightarrow{k_3} CO(a^3\Pi) + \text{photon} \quad (10)$$

$$CO(b^3\Sigma^+) + M \xrightarrow{k_4} CO(a^3\Pi) \quad (11)$$

We have modelled the time-dependent formation of the CO $a^3\Pi$ state using integrated kinetic equations for the species above (provided in the ESI,† along with the rate constants from the literature). The modelling shows that at the pressures of our experiments, the CO $a^3\Pi$ state is formed rapidly, with the collisional quenching steps occurring much faster than CO emission. The fractional yield of the CO $a^3\Pi$ state, relative to the initial number density of the B state, increases from 66% at 25 Torr to 98% at 100 Torr. The natural lifetime for appearance of the CO $a^3\Pi$ state decreases from 5 ns at 25 Torr to less than 2 ns at 100 Torr. The average time between collisions is 4 ns at 25 Torr and 1 ns at 100 Torr. While the formation of the $a^3\Pi$ state occurs rapidly under our conditions, its reaction with ground state CO proceeds slowly (eqn (5)). These results suggest that the long-lived precursor identified by Faust and coworkers in their time-resolved C_2 emission studies is likely the CO $a^3\Pi$ state.[41]

Effect of rotational excitation on CO reactivity

The relative emission intensities in Fig. 5 show that the optical field polarization influences the amount of $C_2(d^3\Pi_g)$ that results from strong field excitation of CO. At the highest powers, we see that multiphoton CO excitation in the dynamic polarization grating yields twice as much C_2 as does excitation in the optical centrifuge. Here we consider the effect of the field polarization

on the multiphoton absorption process and the role of CO rotation on the reactions that form C_2.

The polarization of the optical field does not appear to affect the multiphoton absorption process. Our power-dependent data (Fig. 6) show that CO excitation involves a similar number of photons for both optical polarization schemes. Strickland and coworkers have shown in photodissociation experiments with polarized light that adiabatic alignment in strong fields results in multiphoton absorption with a directionality that follows the field, as long as the field does not vary too quickly.[50] In our experiments using oppositely chirped pulses, molecules aligned in the strong field adiabatically follow the field until the time-dependent polarization frequency varies too quickly. For the optical centrifuge polarization, molecules are spun into high rotational states until the field becomes too weak to trap them or spins too fast for them to keep up. The polarization of the field works together with the molecule's angular momentum to continue to ramp them into higher J states. In the dynamic polarization grating, there is no comparable rotational excitation through alignment in the field. In this case, the field polarization varies between right and left circular, thereby changing the rotational orientation in the field.

The extent of rotational excitation in CO was measured with below threshold excitation using high-resolution transient IR absorption for CO states with $J > 60$. Transient signals for individual CO rotational states were collected at 5 Torr to avoid interference from C_2 emission. Fig. 8a shows the C_2 emission thresholds as a function of CO pressure; no emission is observed at pressures below 10 Torr.

For both optical polarizations, a number of CO rotational states with $J = 62$–73 and E_{rot} up to 10 400 cm^{-1} were investigated. The transient signals for CO $J = 70$ are shown in Fig. 8b with the OCP and the DPG. Fig. 8c shows the relative CO populations excited with the OCP and the DPG, based on IR polarization-dependent measurements, where the total relative state-specific population is determined by $S(J) = 2S_{\parallel} + S_{\perp}$. Here, $S_{\parallel}(S_{\perp})$ is the transient signal for parallel (perpendicular) IR detection as described previously.[26,27] For each J state, the CO signals with the OCP are larger by at least a factor of two than those with the DPG. Fig. 8d shows the ratio of $S(J)$ values for OCP and DPG. The ratio increases with J and has an average value of 3.2 for this range of states. These measurements show that the number densities of high-J CO molecules are larger with the OCP. While the OCP traps and spins molecules to high rotational states by the angularly accelerating optical field, the DPG can induce rotational excitation through ladder-climbing Raman transitions based on the oppositely chirped pulses. We attribute the reduced $C_2(d^3\Pi_g)$ yield to the increased number of highly rotationally excited CO molecules made with the OCP.

Molecules in extreme rotational states have rotational periods (t_{rot}) that can be much shorter than the duration of a collision (t_{col}), thereby reducing the effectiveness of collisional energy transfer and bimolecular reactions. This idea is at the heart of the rotational adiabaticity parameter, which is defined as $a = t_{col}/t_{rot}$. A simple rigid rotor model indicates that CO($J = 70$) has an adiabaticity parameter of $a = 6$, based on 300 K collision velocities. This situation is the opposite of the sudden approximation, where rotation is considered fixed relative to the collision. The sudden approximation is commonly used in calculations of reaction rates. Being able to prepare molecules with very large amounts of rotational energy using an optical centrifuge provides us the opportunity to explore collisional behaviour under rotationally adiabatic conditions.

Previous studies in our laboratory have shown the importance of rotational adiabaticity in the collisional relaxation of optically centrifuged CO_2($J = 100$) with Ar and He. With its small mass,

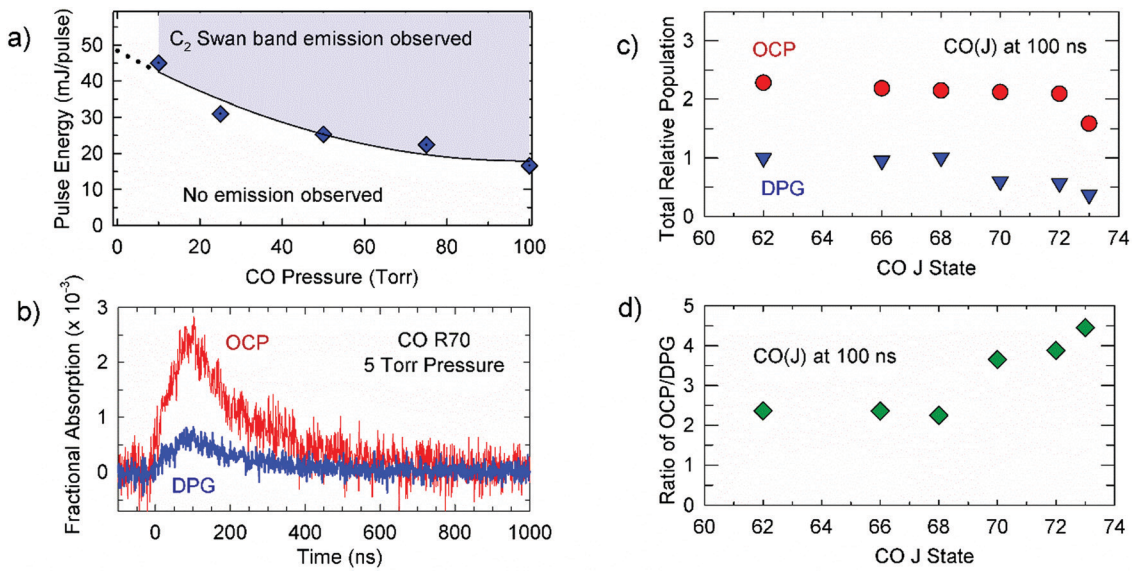

Fig. 8 (a) The pressure dependence of the Swan band emission threshold. (b) R-branch high-resolution transient IR absorption for the CO $J = 70$ state with OCP and DPG excitation. (c) J-Dependent transient intensities at 100 ns based on polarization-sensitive IR detection. (d) Ratio of $S(J)$ values with OCP and DPG.

helium has very short collision times relative to the $CO_2(J = 100)$ rotational period. Argon on the other hand has collision times with CO_2 that are 2.5 times longer than He/CO_2 collisions. We find that He is significantly more effective than Ar at quenching $CO_2(J = 100)$, despite having similar scattering cross sections.[28] We speculate that similar dynamics could well be involved in the bimolecular reactions of CO when its excitation includes large amounts of rotational energy. These processes will be the subject of future investigations.

Conclusions

Here, we have used strong optical fields based on shaped chirped pulses to excite CO *via* multiphoton absorption and investigate how CO rotation affects the yield of bimolecular reactions that form C_2. The observation of Swan band emission initiated by the strong field pulse shows that $C_2(d^3\Pi_g)$ is produced from bimolecular reactions of excited CO. Kinetic modelling using known collisional quenching rates and emission lifetimes suggests that the CO $a^3\Pi$ state is a likely reactant candidate. We see that larger number densities of rotationally excited CO (with $J > 60$) are made with the optical centrifuge than with the dynamic polarization grating. Reduced intensity for Swan band emission indicates that fewer C_2 molecules are formed with the optical centrifuge. Based on these findings, we attribute the reduced C_2 yield to the presence of large amounts rotational energy in the CO reactants. These studies show how strong optical fields from shaped pulses can induce new types of chemistry and we hope that these results will motivate new theoretical studies of such processes.

Conflicts of interest

There are no conflicts to declare.

Acknowledgements

The authors are grateful to Profs John T. Fourkas and R. W. Field for many fruitful discussions on polarization effects and CO photophysics, respectively. Financial support from the National Science Foundation (NSF CHE-1058721 and CHE-1800531) and the University of Maryland is gratefully acknowledged.

Notes and references

1 G. O. Sitz and R. L. Farrow, *J. Chem. Phys.*, 1994, **101**, 4682–4687.
2 H. Stapelfedt and T. Seideman, *Rev. Mod. Phys.*, 2003, **75**, 543–557.
3 D. Teillet-Billy, L. Malegat, J. P. Gauyacq, R. Abouaf and C. Benoit, *J. Phys. B: At., Mol. Opt. Phys.*, 1989, **22**, 1095–1102.
4 J. P. Cryan, P. H. Bucksbaum and R. N. Coffee, *Phys. Rev. A: At., Mol., Opt. Phys.*, 2009, **80**, 063412.
5 K. Kitano, H. Hasegawa and Y. Ohshima, *Phys. Rev. Lett.*, 2009, **103**, 223002.
6 S. Fleischer, Y. Khodorkovsky, Y. Prior and I. S. Averbukh, *New J. Phys.*, 2009, **11**, 105039.
7 C. Vallance, *Phys. Chem. Chem. Phys.*, 2011, **13**, 14427–14441.
8 G. Karras, M. Ndong, E. Hertz, D. Sugny, F. Billard, B. Lavorel and O. Faucher, *Phys. Rev. Lett.*, 2015, **114**, 103001.
9 H. Hou, Y. Huang, S. J. Gulding, C. T. Rettner, D. J. Auerbach and A. M. Wodtke, *Science*, 1999, **284**, 1647–1650.
10 A. Baltuska, Th. Udem, M. Uiberacker, M. Hentschel, E. Goulielmakis, Ch. Gohle, R. Holzwarth, V. S. Yakovlev, A. Scrinzi, T. W. Hansch and F. Krausz, *Nature*, 2003, **421**, 611–615.
11 V. A. Alekseev, J. Grosser, O. Hoffmann and F. Rebentrost, *J. Chem. Phys.*, 2008, **129**, 201102.
12 F. F. Crim, *PNAS*, 2008, **105**, 12654–12661.
13 J. P. Palastro, J. Penano, L. A. Johnson and B. Hafizi, *Phys. Rev. A*, 2016, **94**, 023816.
14 Y. Miyamoto, H. Hara, T. Hiraki, T. Masuda, N. Sasao, S. Uetake, A. Yoshimi, K. Yoshimura and M. Yoshimura, *J. Phys. B: At., Mol. Opt. Phys.*, 2018, **51**, 015401.
15 A. D. Rudert, J. Martin, W.-B. Gao, J. B. Halpern and H. Zacharias, *J. Chem. Phys.*, 1999, **111**, 9549–9559.
16 Y. Ohshima and H. Hasegawa, *Int. Rev. Phys. Chem.*, 2010, **29**, 619–663.
17 O. Korech, U. Steinitz, R. J. Gordon, I. S. Averbukh and Y. Prior, *Nat. Photonics*, 2013, **7**, 711–714.
18 E. Gershnabel and I. S. Averbukh, *Phys. Rev. Lett.*, 2018, **120**, 083204.
19 J. Karczmarek, J. Wright, P. Corkum and M. Ivanov, *Phys. Rev. Lett.*, 1999, **82**, 3420–3423.
20 J. Li, J. T. Bahns and W. C. Stwalley, *J. Chem. Phys.*, 2000, **112**, 6255–6261.
21 L. W. Yuan, C. Toro, M. Bell and A. S. Mullin, *Faraday Discuss.*, 2011, **150**, 101–111.
22 L. Yuan, S. W. Teitelbaum, A. Robinson and A. S. Mullin, *Proc. Natl. Acad. Sci. U. S. A.*, 2011, **108**, 6872–6877.
23 C. Toro, Q. N. Liu, G. O. Echebiri and A. S. Mullin, *Mol. Phys.*, 2013, **111**, 1892–1901.
24 M. J. Murray, H. M. Ogden, C. Toro, Q. N. Liu, D. A. Burns, M. H. Alexander and A. S. Mullin, *J. Phys. Chem. A*, 2015, **119**, 12471–12479.
25 M. J. Murray, H. M. Ogden, C. Toro, Q. N. Liu and A. S. Mullin, *Chem. Phys. Chem.*, 2016, **17**, 3692–3700.
26 M. J. Murray, H. M. Ogden and A. S. Mullin, *J. Chem. Phys.*, 2017, **147**, 154309.
27 M. J. Murray, H. M. Ogden and A. S. Mullin, *J. Chem. Phys.*, 2018, **148**, 084310.
28 A. A. Milner, A. Korobenko, J. W. Hepburn and V. Milner, *J. Chem. Phys.*, 2017, **147**, 124202.
29 D. Gerlich and T. Rox, *Z. Phys. D: At., Mol. Clusters*, 1989, **13**, 259–268.
30 A. Gonzalez Urena, M. Menendez, A. Sole Sabate and A. Aguilar Navarro, *Chem. Phys. Lett.*, 1991, **176**, 315–321.
31 A. A. Viggiano and R. A. Morris, *J. Phys. Chem.*, 1996, **100**, 19227–19240.
32 T. Glenewinkel-Meyer and D. Gerlich, *Isr. J. Chem.*, 1997, **37**, 343–352.
33 K. Nobusada, K. Moribayashi and H. Nakamura, *Faraday Trans.*, 1997, **93**(5), 721–726.

34 L. Paetow, F. Unger, W. Beichel, G. Frenking and K. Weitzel, *J. Chem. Phys.*, 2010, **132**, 174305.
35 Y. Xu, B. Xiong, Y. C. Chang and C. Y. Ng, *J. Chem. Phys.*, 2012, **137**, 241101.
36 R. Welsch and U. Manthe, *J. Chem. Phys.*, 2014, **141**, 051102.
37 R. Liu, F. Wang, B. Jiang, G. Czako, M. Yang, K. Liu and H. Guo, *J. Chem. Phys.*, 2014, **141**, 074310.
38 H. Song and H. Guo, *J. Chem. Phys.*, 2014, **141**, 244311.
39 T. Uhlemann, J. Wallauer and K. Weitzel, *Phys. Chem. Chem. Phys.*, 2015, **17**, 16454–16461.
40 G. Herzberg, *Phys. Rev.*, 1946, **70**, 762–764.
41 W. L. Faust, L. S. Goldberg, B. B. Craig and R. G. Weiss, *Chem. Phys. Lett.*, 1981, **83**, 265–269.
42 M. Alden, S. Wallin and W. Wendt, *Appl. Phys. B: Photophys. Laser Chem.*, 1984, **33**, 205–208.
43 J. E. M. Goldsmith and D. Therese Biernacki Kearsley, *Appl. Phys. B: Photophys. Laser Chem.*, 1990, **50**, 371–379.
44 H. L. Wallaart, B. Piar, M.-Y. Perrin and J.-P. Martin, *Chem. Phys. Lett.*, 1995, **246**, 587–593.
45 Yu. Z. Ionikh, I. N. Kostyukevich and N. V. Chernysheva, *Opt. Spectrosc.*, 1996, **80**, 590–594.
46 A. Tanabashi, T. Hirao, T. Amano and P. F. Bernath, *Astrophys. J., Suppl. Ser.*, 2007, **169**, 472–484.
47 G. M. Grigorian and A. Cenian, *IOP Conf. Ser.: Mater. Sci. Eng.*, 2014, **62**, 1–5.
48 J. Rosell, J. Sjoholm, M. Ritcher and M. Alden, *Appl. Spectrosc.*, 2013, **67**, 314–320.
49 E. E. Ivanov, Yu. Z. Ionikh, N. P. Penkin and N. V. Chernysheva, *Sov. J. Chem. Phys.*, 1991, **7**, 2989.
50 P. Dietrich, D. T. Strickland, M. Laberge and P. B. Corkum, *Phys. Rev. A: At., Mol., Opt. Phys.*, 1993, **47**, 2305.

